ACS Catalysis

Universitat d'Alacant
Universidad de Alicante

Subscriber access provided by Universidad de Alicante

Article

Role of hydroxyl groups in the preferential oxidation of CO over copper oxide-cerium oxide catalysts

Arantxa Davó-Quiñonero, Miriam Navlani-García, Dolores Lozano-Castello, Agustín Bueno-López, and James A. Anderson

ACS Catal., **Just Accepted Manuscript** • DOI: 10.1021/acscatal.5b02741 • Publication Date (Web): 01 Feb 2016

ACS Publications

ACS Catalysis is published by the American Chemical Society. 1155 Sixteenth Street N.W., Washington, DC 20036

Role of hydroxyl groups in the preferential oxidation of CO over copper oxide-cerium oxide catalysts

Arantxa Davó-Quiñonero[1], *Miriam Navlani-García*[1], *Dolores Lozano-Castelló*[1,2], *Agustín Bueno-López*[1,2,*], *James A. Anderson*[2]

[1]MCMA group. Inorganic Chemistry Department; University of Alicante.

[2]Surface Chemistry and Catalysis Group, School of Engineering, University of Aberdeen.

KEYWORDS. PROX; copper; ceria, CO oxidation; H_2 purification.

ABSTRACT

Model $CuO/Ce_{0.8}X_{0.2}O_{\delta}$ catalysts (with X = Ce, Zr, La, Pr or Nd) have been prepared in order to obtain CuO/ceria materials with different chemical features, and have been characterized by XRD, Raman spectroscopy, N_2 adsorption and H_2-TPR. CO-PROX experiments have been performed in a fixed-bed reactor and in an *operando* DRIFTS cell coupled to a mass spectrometer. The CO oxidation rate over CuO/Ceria catalysts correlates with the formation of the Cu^+-CO carbonyl above a critical temperature (90ºC for the experimental conditions in this study) because copper-carbonyl formation is the rate limiting step. Above this temperature CO oxidation capacity depends on the redox properties of the catalyst. However, decomposition of adsorbed intermediates is the slowest step below this threshold temperature. The hydroxyl groups on the catalyst surface play a key role in determining the nature of the carbon-based intermediates formed upon CO chemisorption and oxidation. Hydroxyls favor the formation of bicarbonates with respect to carbonates, and catalyst forming more bicarbonates produce faster CO oxidation rates than those which favor carbonates.

1.- Introduction

CO oxidation by molecular oxygen is probably one of the most studied catalyzed reactions, and the selective oxidation of CO in H_2-rich gas mixtures (CO-PROX) has become of special relevance in recent years in order to provide sufficiently pure H_2 for proton exchange membrane fuel cells (PEMFC).[1,2] H_2 is obtained by catalytic reforming of hydrocarbons followed by the water gas shift reaction (WGS),[3] and this process yields a H_2-rich gas stream with up to 1% of CO. This high concentration is not acceptable because CO poisons the Pt electrocatalysts, and CO concentration must be lowered below *ca.* 100 ppm.[4] The CO-PROX reaction is one of the most suitable methods for the purification of such H_2-rich gas streams, and copper oxide-cerium oxide catalysts are promising materials[5-8] for CO-PROX that could replace expensive Pt or Au catalysts.[9-13]

The CO-PROX reaction is a competitive process where CO and H_2 compete with each other for molecular oxygen[14]. The catalyst must be selective towards the CO-O_2 reaction with regard to the undesired oxidation of H_2, which decreases the net H_2 yield of the complete catalytic reforming + WGS + CO-PROX series of reactions. A correlation was established between the CO oxidation rate and the level of interfacial reduction of Cu^{2+} to Cu^{+}, and such interfacial reduction can be correlated to the formation of Cu^{+}-CO carbonyls.[15,16] On the other hand, the oxidation of H_2 occurs once copper is significantly reduced, and the active species for the H_2-O_2 reaction are partially reduced copper oxide nanoparticles[15] where dissociative chemisorption of H_2 takes place.[17] The selectivity of copper oxide-cerium oxide catalysts can be related to the preferential adsorption of CO on Cu^{+} and hindered H_2 dissociation on oxidized sites.[17]

The evolution of the carbon-containing species on the catalysts surface during the course of the reaction is complex and is not completely understood, but it has been reported that surface hydroxyls on the catalyst have a positive effect on CO oxidation for noble metal catalyst.[18] This aspect has been analyzed in detail in this study for CuO/Ceria, and model CuO/$Ce_{0.8}X_{0.2}O_{\delta}$ catalysts (with X = Ce, Zr, La, Pr or Nd) have been prepared in order to obtain CuO/Ceria materials with different chemical features. The objectives were to understand the role of the carbon containing intermediates in the CO oxidation reaction, and to determine whether the hydroxyl groups on the catalyst influence the formation of bicarbonates in preference to carbonates, and to provide evidence to support a hypothesis that catalysts which preferentially form bicarbonates are able to oxidize CO faster than those forming carbonates-type species.

2.- Experimental

2.1 Catalysts preparation.

Five metal oxides with composition $Ce_{0.8}X_{0.2}O_{\delta}$ (X = Ce, Zr, La, Pr or Nd) were prepared using the following metal precursors: $Ce(NO_3)_3 \cdot 6H_2O$ (Alfa-Aesar, 99.5 %), $ZrO(NO_3)_2 \cdot xH_2O$ (Fluka, ~ 27 % Zr), $La(NO_3)_3 \cdot 6H_2O$ (≥ 99.0%), $Pr(NO_3)_3 \cdot 6H_2O$ (99.9%) and $Nd(NO_3)_3 \cdot 6H_2O$ (≥ 99.9%).

The amounts of each precursor used were those required to obtain 5 g of metal oxide, and aqueous solutions of these amounts were prepared with 10 ml of solvent. The dissolutions were introduced in a muffle furnace previously heated at 200ºC, and after 1 hour, the temperature was increased at 10ºC/min until 500ºC, holding the samples at this temperature for 2 hours.

$CuO/Ce_{0.8}X_{0.2}O_{\delta}$ catalysts were prepared afterwards with a 5 wt. % target Cu loading. The required amount of $Cu(NO_3)_2 \cdot 5 \cdot (1/2)H_2O$ (Sigma Aldrich, 98 %) was dissolved in 2 ml of water and 2.5 g of $Ce_{0.8}X_{0.2}O_{\delta}$ was impregnated with this solution. The impregnated supports were heat treated following the same protocol used for the supports preparation, that is, they were introduced in a muffle furnace previously heated at 200ºC, and after 1 h, the temperature was increased at 10ºC/min until 500ºC, holding this temperature for 2 h.

2. 2. Catalysts characterization.

X-ray diffractograms were obtained in a Bruker D8 advance diffractometer, using CuKα radiation (λ=0.15418 nm) between 10 and 90º (2θ), with a step of 0.02º and a time of 3 s per step. The average crystallite size of the mixed oxide supports was determined using the Williamson-Hall's equation.[19]

N_2 adsorption isotherms were performed at −196ºC in an automatic volumetric system (Autosorb-6, Quantachrome) after the catalysts were degassed at 150ºC for 4 h. The specific surface areas, pore volumes and pore sizes were determined with the BET, DR and BJH methods, respectively.

Raman spectra were recorded in a Bruker RFS 100/S Fourier Transform Raman Spectrometer with a variable power Nd-YAG laser source (1064 nm). The spectra shown in this document were normalized by dividing the intensity of each spectrum by the intensity of its F_{2g} band maximum.

The catalysts were characterized by Temperature Programmed Reduction with H_2 (H_2-TPR) in a ThermoQuest device (LE instruments), consisting of a tubular quartz reactor coupled to a

thermal conductivity detector (TCD). The experiments were conducted with 50 mg of catalyst. The temperature was raised at 10ºC·min^{-1} from room temperature to 900ºC and a 30 mL·min^{-1} flow of 5 vol % H_2 in N_2 was used. A CuO reference sample was used to quantify the amount of H_2 consumed in the experiments, and two parameters were calculated:

$$H_{2\ consumed}\ mol / CuO\ mol = \frac{H_2\ mol\ consumed}{CuO\ mol}$$

where "H_2 mol consumed" are the total moles of H_2 consumed in a certain H_2-TPR experiment and "CuO mol" are the CuO mol on the parcel of catalyst used in that H_2-TPR experiment. The H_2 mol consumed by the catalysts were calculated integrating the area under the TCD signal profiles, and converting these areas into H_2 mole considering the area of the reduction peak obtained with the reference CuO sample and assuming total reduction to Cu^0.

$$Ce^{4+}\ reduced\ (\%) = 100 \cdot \frac{2 \cdot (H_2\ mol\ consumed - H_2\ mol\ for\ CuO\ reduction)}{Ce\ moles}$$

where "H_2 mol for CuO reduction" are the moles of H_2 required for all CuO in the sample of catalyst to be reduced to Cu^0 and "Ce moles" are the total moles of Ce in the sample of catalyst.

2.3. Catalytic tests in a fixed-bed reactor.

Catalytic tests were carried out in a U-shape quartz reactor (16 mm inner diameter) with 150 mg of catalyst and 100 mL/min (30000 h^{-1}) of a gas mixture with 2 % CO, 2 % O_2 and 30 % H_2 balanced with He. The gas stream was fed to the reactor by means of mass flow controllers (Bronkhorst). The gas composition was monitored after the reaction with a gas chromatograph

Agilent Technologies 6890N, equipped with a CRT column operating at 80 ºC and a TCD detector.

Variable temperature and isothermal experiments were carried out. In variable temperature experiments, the temperature was raised at 2ºC/min until reaching 200ºC. Consecutive ramp experiments were performed with selected catalysts using the same aliquot of sample. After the first ramp, the catalyst was reoxidized at 200ºC in 10 %O_2/He flow for 1 h and then cooled to room temperature in inert gas. Then, the reaction gas mixture was fed to the reactor and the temperature was raised at 2ºC/min until 200ºC, repeating this protocol four times. After the fourth run, the catalysts were reoxidized and cooled as described, and a fifth heating step was carried out with the reaction gas mixture, but in this case the temperature was stabilized at 120ºC and the selected catalysts were held under these reaction conditions for 12 h in order to evaluate the long-term stability.

CO conversion and selectivity were calculated as follows:

$$\text{CO conversion (\%)} = \frac{P_{CO}^{in} - P_{CO}^{out}}{P_{CO}^{in}} \cdot 100 \qquad \text{CO selectivity (\%)} = \frac{P_{CO}^{in} - P_{CO}^{out}}{P_{O_2}^{in} - P_{O_2}^{out}} \cdot 50$$

where P_{CO}^{in} and P_{CO}^{out} are the inlet and outlet CO partial pressures, respectively, and $P_{O_2}^{in}$ and $P_{O_2}^{out}$ are the O_2 partial pressures.

2.4. Operando DRIFTS-MS experiments.

The reaction mechanism was studied in a Shimadzu (IR Tracer-100) Fourier Transform Infrared Spectrometer with a Harrick reaction cell coupled to a EcoSys-P mass spectrometer. The reaction cell was designed to allow the reaction gas mixture (2 % CO, 2 % O_2 and 58 % H_2

balanced with He; 50 ml/min) to pass through the catalyst bed (100 mg without any diluent) with the gas exit at the bottom.

The catalysts were first pretreated at 400ºC for 15 min in a flow of air, and the reaction cell was cooled afterwards to room temperature while maintaining the air flow. A background spectrum was recorded for each catalyst at room temperature after this cleaning step, and then, air was replaced by the reaction gas mixture and the temperature was raised at 5ºC/min while infrared spectra were recorded at 10ºC intervals. Each spectrum was obtained as an average of 75 scans, in the range 4000 to 1000 cm^{-1} with a resolution of 2 cm^{-1}. The background spectrum of each catalyst was subtracted from those obtained under reaction conditions, and therefore, the features observed can be attributed to species formed or depleted during the reaction rather than to the catalysts structure.

3.- Results and discussion

3.1. Catalysts characterization by N_2 adsorption, XRD and Raman spectroscopy.

The crystalline structure and porosity of the catalysts was characterized by XRD, N_2 adsorption, and Raman spectroscopy. The X-ray diffractograms are compiled in Figure 1 and the crystallite sizes and cell parameters calculated for the ceria-based supports are compiled in Table 1.

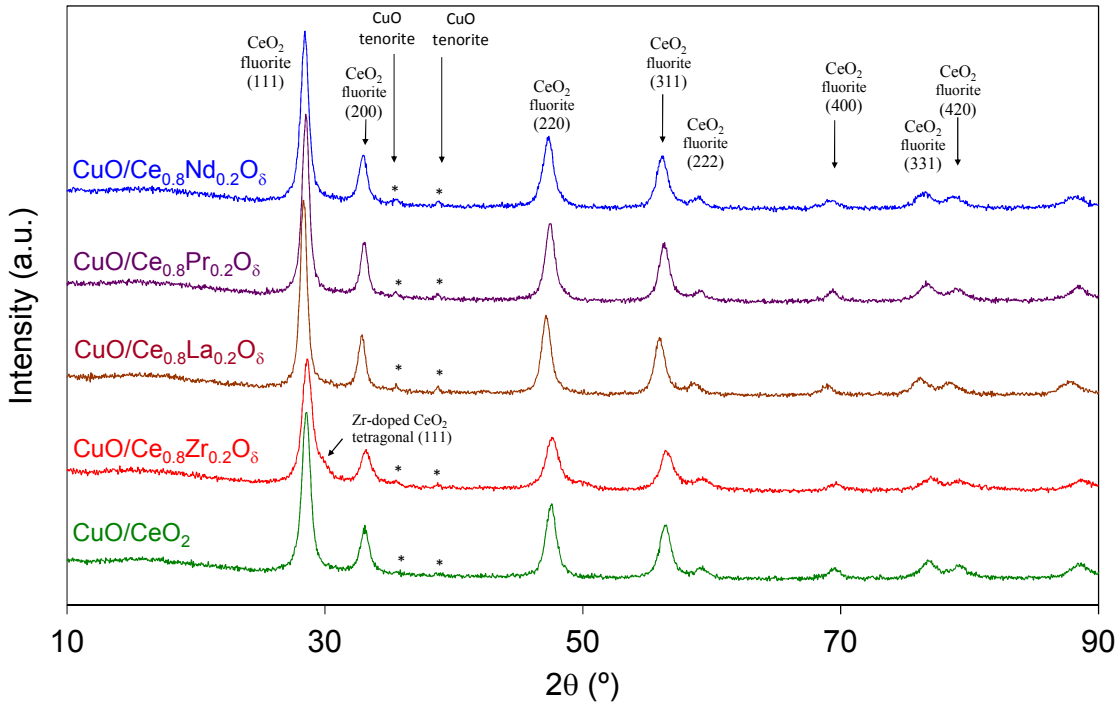

Figure 1. X-Ray diffractograms of the catalysts.

All diffractograms show the typical reflexions of the fluorite structure of ceria, and also tiny peaks of CuO at 35.7 and 39.0º seem to be present in most catalyst. Evidence of other crystalline phases are only identified for the $CuO/Ce_{0.8}Zr_{0.2}O_{\delta}$ catalyst, which shows a shoulder at lower angles of the (111) fluorite peak at 29.0º that is consistent with the presence of a Zr-rich tetragonal phase (peak 111). Evidence of segregated phases of La, Pr or Nd was not observed in the diffractograms.

Table 1. Results of the catalysts characterization by N_2 adsorption, XRD and Raman spectroscopy.

Catalyst	BET (m^2/g)	Pore volume DR (cm^3/g)	Pore size BJH (nm)	Crystallite size (nm)	Cell parameter (nm)	F_{2g} band Raman shift (cm^{-1})
CuO/CeO_2	58	0.021	12	13	0.5407	441
$CuO/Ce_{0.8}Zr_{0.2}O_\delta$	60	0.020	12	13	0.5392	457
$CuO/Ce_{0.8}La_{0.2}O_\delta$	40	0.015	17	26	0.5448	446
$CuO/Ce_{0.8}Pr_{0.2}O_\delta$	35	0.013	12	27	0.5411	450
$CuO/Ce_{0.8}Nd_{0.2}O_\delta$	45	0.016	12	16	0.5429	453

The cell parameter calculated for the ceria bare support (0.5407 nm) is consistent with values typically obtained for this material,[20] and doping with some cations affect this value. The cell parameter does not change significantly upon ceria doping with Pr, which is not surprising because the sizes of the Ce cations (0.097 nm for Ce^{4+} and 0.114 nm for Ce^{3+}) are almost equal to those of Pr cations (0.096 nm for Pr^{4+} and 0.113 nm for Pr^{3+}).[21] On the contrary, Zr doping decreases the cell parameter of ceria while doping with La or Nd increases the cell parameter. The cell parameter contraction upon Zr doping is expected considering the smaller size of Zr^{4+} (0.084 nm) with regard to Ce^{4+}, and the cell expansion upon La or Nd doping is consistent with the larger size of their cations (0.116 nm for La^{3+} and 0.112 nm for Nd^{3+}). These modifications of the cell parameters of ceria upon doping provide evidence that the foreign cations are actually located into the parent ceria framework. However, it cannot be ruled out that, in addition to the amount introduced into the ceria lattice, Zr was partially segregated, since evidence of such segregated phase was observed in the diffractograms.

The pore size (12-17 nm) and pore volume (0.013-0.021 cm^3/g) values are quite similar for all catalysts. The crystallite size of the ceria supports are in the 13-27 nm range (see Table 1), and the smallest sizes are obtained for undoped and Zr-doped ceria. These two supports also have the largest specific surface areas (58-60 m^2/g), with these values being in good agreement with those typically obtained for cerium oxides exposed to a similar thermal history.[20] Ceria doping with La, Pr or Nd leads to a decrease of the specific surface area and an increase of the crystallite size, which means that these dopants facilitate sintering. It is known that the effect of dopants on ceria sintering depends on the temperature of the thermal treatments.[22] As a rule of thumb, dopants partially hinder ceria sintering for high temperature calcination (above 800-900ºC) while they have no effect or promote sintering for mild temperature calcination (500-600ºC). The argument postulated to explain such behavior is that the surface defects created upon doping decrease the energy required for crystals to merge, and therefore dopants promote sintering if there are energy restrictions, as occurring at mild temperature. On the contrary, if the temperature is high enough to overcome such energy restrictions to sintering, the effect of dopants is the opposite, partially hindering sintering because they do not allow long-range structural order into the ceria crystals.

Raman spectroscopy (Figure 2) provides additional information about the structure of the catalysts.

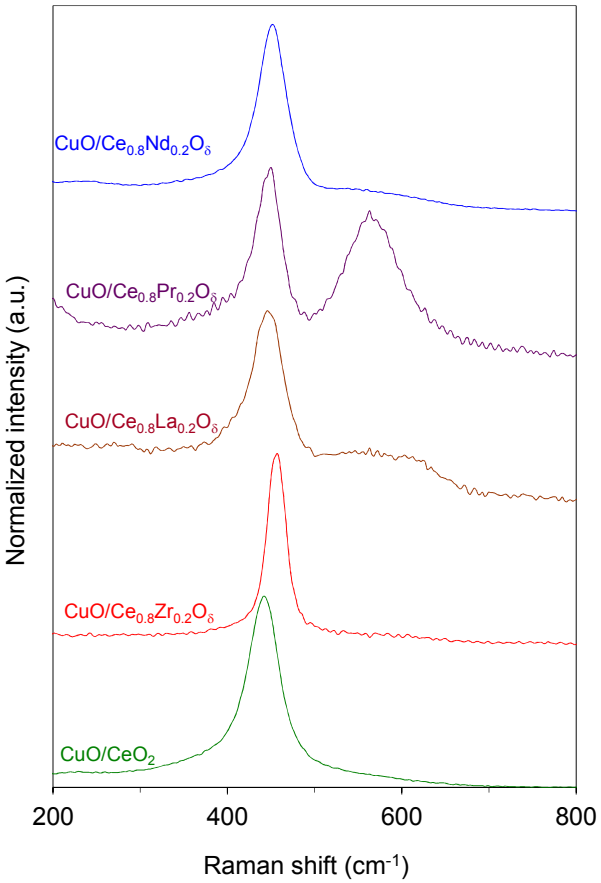

Figure 2. Raman spectra of the catalysts. The spectra were normalized by dividing the intensity of each spectrum between the intensity of its F2g band maximum.

All catalysts show the F_{2g} band around 450 cm^{-1}, which is a typical feature of the ceria-based oxides.[23,24] This band has been attributed to the oxygen breathing frequency around the Ce^{4+} cations.[25,26] The position of this band provides information about the introduction of foreign cations into the ceria lattice. The position of the F_{2g} band in pure ceria is usually ca 464 cm^{-1},[20] and the position obtained for all $CuO/Ce_{0.8}X_{0.2}O_{\delta}$ catalysts is well below this value (see data in Table 1). The shift of the F_{2g} band towards low values is attributed to the presence of foreign

cations into the lattice larger than Ce^{4+}, while the shift towards high values is assigned to the presence of smaller cations. Therefore, the low values obtained for our catalysts suggest the presence of large cations. In the CuO/CeO_2 catalyst, the large cations could be Ce^{3+} and a potential explanation would be that the energy of the laser used to obtain the Raman spectra is sufficiently high to partially reduce the surface. Copper seems to play a key role in this reduction, because this effect is not observed in copper-free ceria catalysts.[20] In catalysts with dopants larger than Ce^{4+}, like La^{3+}, Pr^{3+} and Nd^{3+}, the shift of the F_{2g} band below 464 cm^{-1} must be additionally attributed to the introduction of such cations into the ceria lattice. It is also reasonable to think that Ce^{4+} reduction (and also Pr^{4+} in the case of $CuO/Ce_{0.8}Pr_{0.2}O_{\delta}$) is additionally taking place.

In addition to the F_{2g} band, another band or shoulder appears in some Raman spectra at 540 cm^{-1}, which has been assigned to oxygen vacancies. The relative intensity of this band with regard to the maximum of the F_{2g} band is highest for the Pr-containing catalyst, being much lower for the La- or Nd-doped catalysts and negligible for the remaining samples. The formation of oxygen vacancies is expected upon Ce^{4+} substitution by trivalent cations, like La^{3+} or Nd^{3+}, while is not expected to be relevant upon isovalent substitution of Ce^{4+} by Zr^{4+}. The prominent vacants band observed in $CuO/Ce_{0.8}Pr_{0.2}O_{\delta}$ has been attributed to the easy reduction of the Pr^{4+} cations, which could be even reduced due to the local heating produced by the laser used to excite the samples and obtain the Raman spectra, as previously reported.[21] The presence of Ce^{3+} cations, as previously proposed considering the position of the F_{2g} band, is also expected to lead to the formation of oxygen vacancies. However, the band due to these vacancies is negligible in spectra of CuO/CeO_2, for instance, suggesting that the partial reduction of Ce^{4+} under measurements conditions is high enough to shift the position of the F_{2g} band but not for the band

due to the vacancies to grow. This is not surprising because, usually, the position of the Raman bands is much more sensitive to changes in the physical chemical features of solids than the intensity of the bands, which is affected by other variables like crystal size or radiation absorption.

In conclusion, these characterization results confirm that, in the $CuO/Ce_{0.8}X_{0.2}O_{\delta}$ catalysts prepared, the doping cations are actually located into the parent ceria framework. Only the $CuO/Ce_{0.8}X_{0.2}O_{\delta}$ catalyst shows certain evidences of the formation of a segregated Zr rich phase, but even in this case, it can be confirmed that part of the Zr dopant is located into the ceria lattice.

3.2 Catalysts characterization by H_2-TPR.

The TCD signals monitored during the H_2-TPR experiments are plotted on Figure 3, and all catalysts show a main feature in the 120-300ºC range, which consist of double peaks or a main peak with a shoulder at low temperature. Also, a small band is shown in some profiles around 800ºC, which can be assigned to the reduction of the particles bulk.

The position of the low-temperature reduction bands indicates that $CuO/Ce_{0.8}Zr_{0.2}O_{\delta}$ and CuO/CeO_2 are reduced at the lowest temperature, and that the behavior of these two catalysts is quite similar to each other.

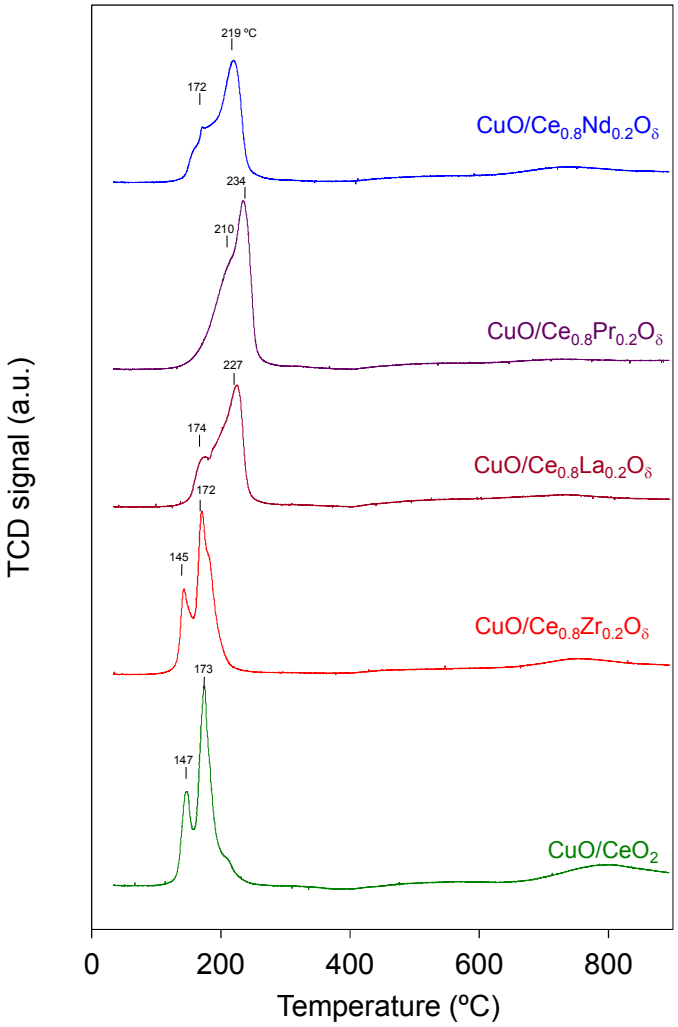

Figure 3. H_2-TPR profiles of the catalysts.

Different events are taking place within the reduction bands in the 120-300ºC range, and the dual-mode shape reported for MO/CeO_2 catalysts (MO = Metal Oxide) has been related to the reduction of the supported metal oxide (MO) and ceria in close contact with MO at the lowest temperature, and to surface ceria reduction which is not directly in contact with MO at higher temperature.[27] In the case of CuO catalysts, the reduction of Cu^{2+} to Cu^0 in two consecutive steps, Cu^{2+} to Cu^+ first and Cu_+ to Cu^0 afterwards cannot be ruled out. In the $CuO/Ce_{0.8}Pr_{0.2}O_\delta$ catalyst it must be additionally taken into account that Pr^{4+} is also reduced to Pr^{3+}.

Quantitative values calculated from the H_2-TPR experiments are compiled in Table 2:

Catalyst	$H_{2\ consumed}$ mol/CuO mol	Ce^{4+} reduced (%)
CuO/CeO_2	1.7	20
$CuO/Ce_{0.8}Zr_{0.2}O_\delta$	1.6	22
$CuO/Ce_{0.8}La_{0.2}O_\delta$	1.6	23
$CuO/Ce_{0.8}Pr_{0.2}O_\delta$	1.9	27[a]
$CuO/Ce_{0.8}Nd_{0.2}O_\delta$	1.8	28

Table 2. Quantitative values calculated from the H_2-TPR experiments.

[a]In the $CuO/Ce_{0.8}Pr_{0.2}O_\delta$ catalyst, the percentage of Ce^{4+} reduced is actually $Ce^{4+} + Pr^{4+}$.

In all cases, the moles of H_2 consumed are higher than those of CuO on the catalysts, and this provides experimental evidence that not only is CuO being reduced but also the ceria supports. Considering total reduction of Cu^{2+} to Cu^0, the percentages of Ce^{4+} reduced to Ce^{3+} are in the 20-28 % range for all catalysts.

These H_2-TPR experiments allow concluding that the presence of dopants affect the reducibility of the CuO-Ceria system, and $CuO/Ce_{0.8}Zr_{0.2}O_\delta$ and CuO/CeO_2 are reduced more easily than the remaining catalysts. This affects the temperature required for catalysts reduction by H_2, but differences in the extent of the reduction are not very relevant once totally accomplished.

3.3. Catalytic tests in a fixed-bed reactor.

Figure 4 shows the oxidation of CO (Figure 4a) and the CO selectivity (Figure 4b) obtained in the fixed-bed reactor PROX experiments, where it is observed that the catalysts with the undoped and Zr-doped supports are active and selective at lower temperature than catalysts containing La, Pr or Nd. Four consecutive experiments were carried out with the most active

catalysts ($CuO/Ce_{0.8}Zr_{0.2}O_{\delta}$ and CuO/CeO_2) and reproducible CO conversion and selectivity profiles were obtained, confirming the high stability of these catalysts under reaction conditions. Isothermal experiments were also performed at 120ºC and constant CO conversion and selectivity values were kept for 12 hours. All these curves are included in the supplementary material.

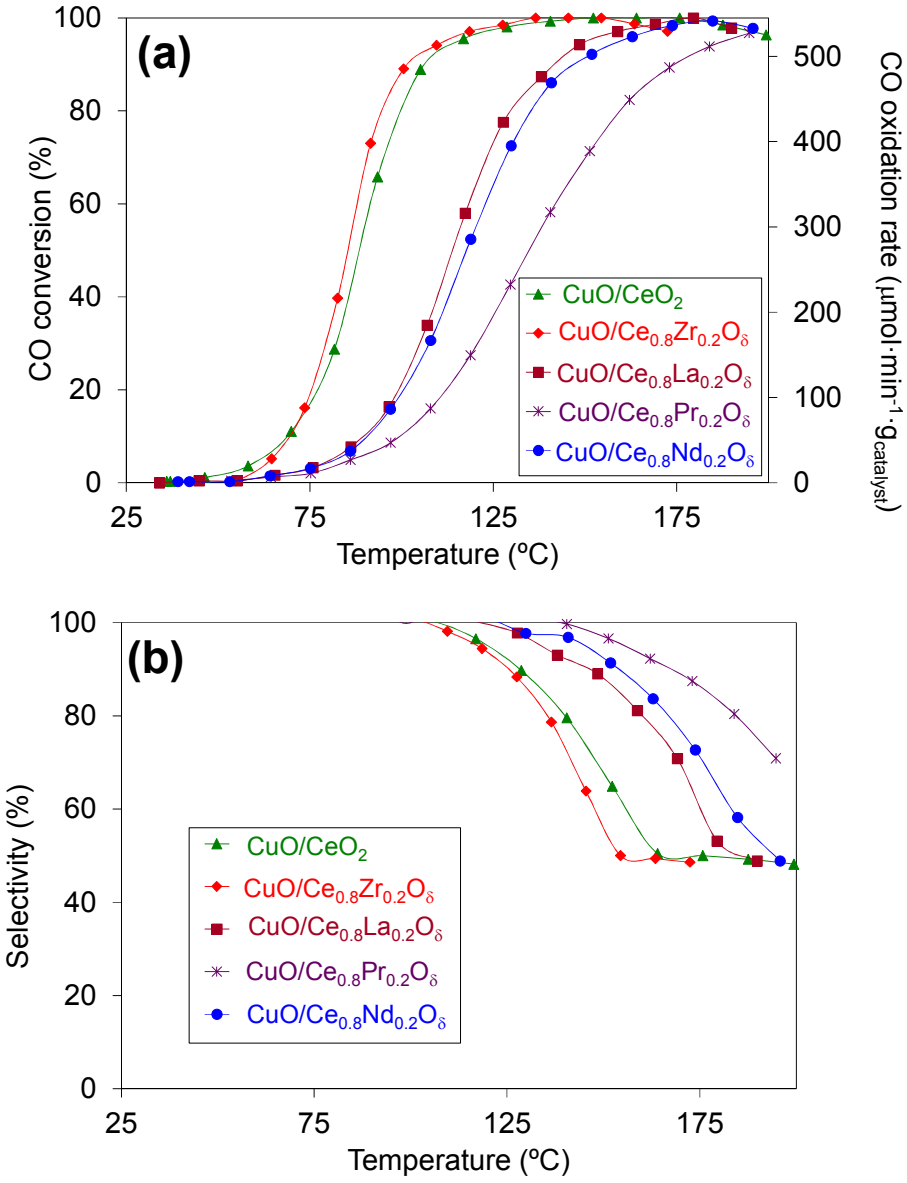

Figure 4. CO-PROX reactions performed in a fixed-bed reactor. (a) CO conversion and oxidation rate and (b) CO selectivity.

The results on Figure 4, together with the previous H_2-TPR characterization, confirm that the reducibility of the catalyst plays an important role in CO oxidation, since the catalytic processes are based on redox cycles taking place on the catalyst surface. In accordance with the well accepted role of the different copper species in the PROX reactions,[15-17] the oxidation of CO starts at temperatures (~ 50ºC) lower than those required for the extensive reduction of the catalyst surface by H_2 (see H_2-TPR in Figure 3). This is in agreement with the hypothesis supporting that the active sites for CO oxidation are Cu^+ sites located at the CuO-Ceria interface. In addition, the selectivity drops (Figure 4b) when temperature approaches the onset temperature for extensive reduction of the catalysts surface (see H_2-TPR in Figure 3), supporting that H_2 oxidation takes place on reduced metal sites.

3.4. *Operando* DRIFTS-MS experiments.

In order to investigate the nature of the carbon intermediates and to determine whether hydroxyl groups on the catalyst play a critical role in the formation of bicarbonates and in the CO oxidation rate, *operando* DRIFTS-MS experiments were carried out.

Figure 5 shows, as representative examples, spectra obtained with $CuO/Ce_{0.8}Zr_{0.2}O_\delta$ and $CuO/Ce_{0.8}La_{0.2}O_\delta$. DRIFT spectra were recorded between 4000-1000 cm^{-1}, but the main features are located in three main regions. Figures 5a and 5d show the 1650-1150 cm^{-1} range, where several vibration/stretching modes corresponding to carbonates, bicarbonates and formates are

identified. Figures 5b and 5e show the 2250-1950 cm^{-1} range, where a single band corresponding to the Cu^{+}-CO carbonyl is observed. Figures 5c and 5d show the 3850-2450 cm^{-1} range, where hydroxyl groups are detected..

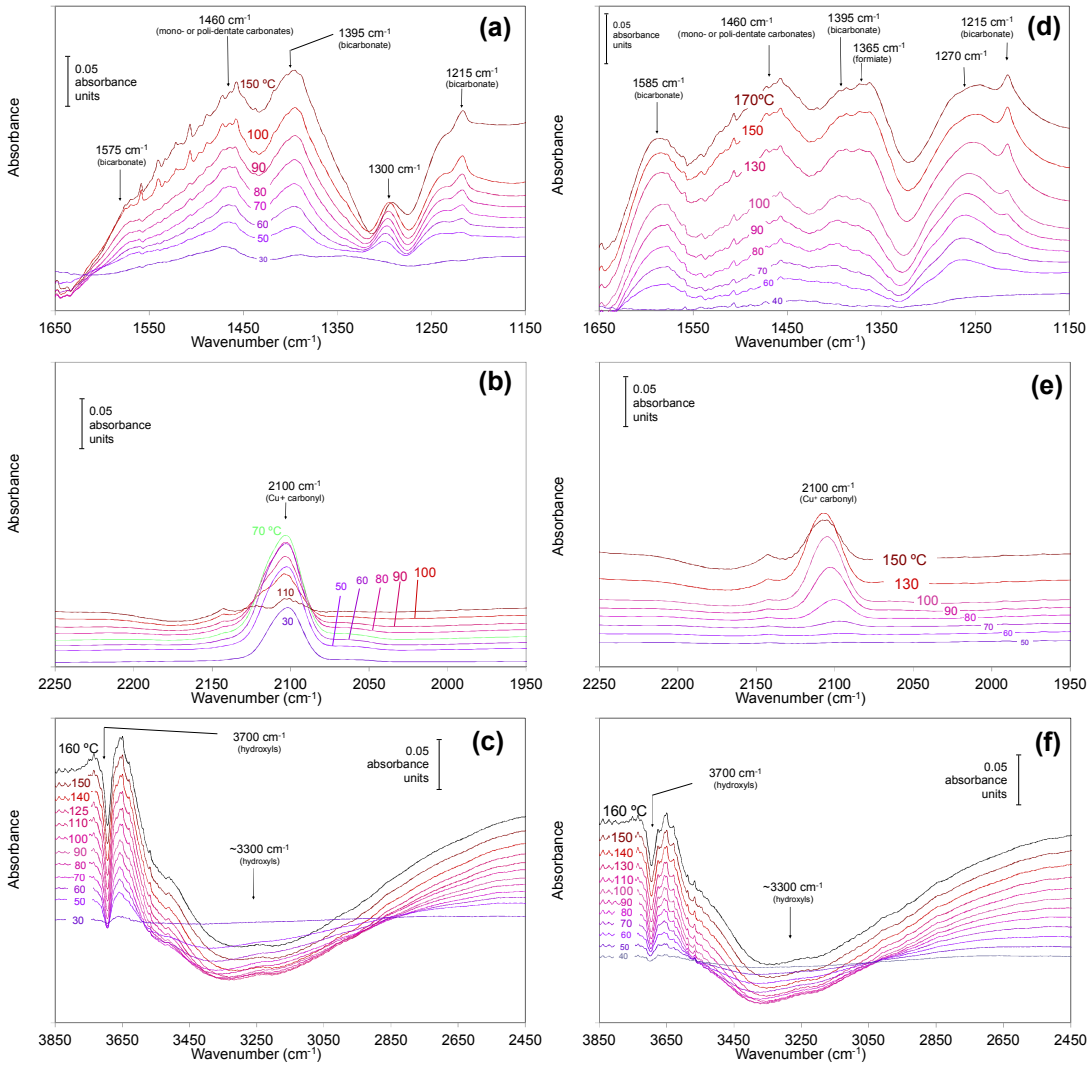

Figure 5. DRIFT spectra as a function of temperature under operando PROX conditions with $CuO/Ce_{0.8}Zr_{0.2}O_{\delta}$ (a, b and c) and $CuO/Ce_{0.8}La_{0.2}O_{\delta}$ (d, e and f).

3.4.1. Role of the catalyst hydroxyls groups

The main carbon-containing reaction intermediates accumulated on the catalysts surface during the PROX reaction are carbonates and bicarbonates, as is observed in the DRIFT spectra (Figure 5). Figure 6 shows the ratio between the band maxima due to bicarbonates (at 1395 cm^{-1}) and carbonates (at 1460 cm^{-1}) as a function of temperature for all catalysts.

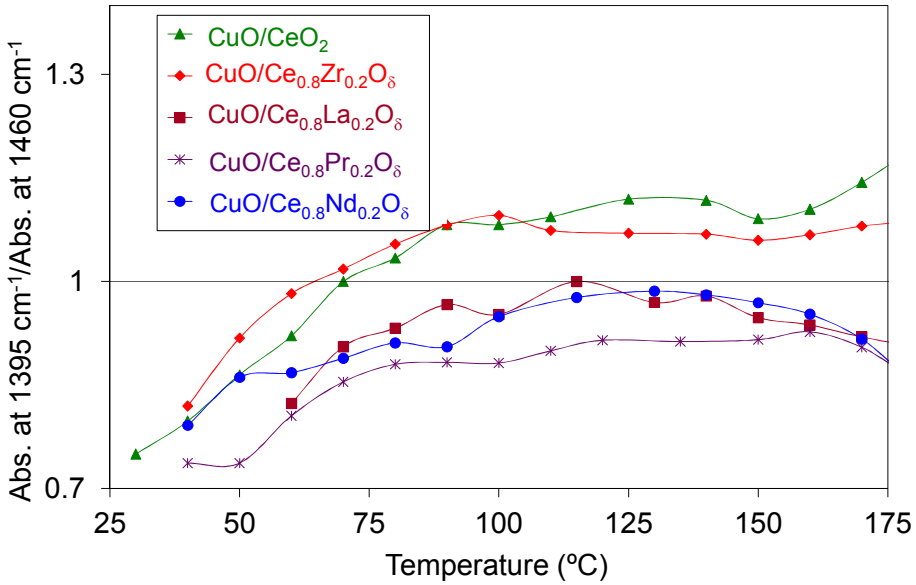

Figure 6. Ratio between the absorbance at 1395 cm^{-1} (bicarbonates) and the absorbance and 1460 cm^{-1} (carbonates) as a function of temperature.

The most active catalysts (CuO/CeO_2 and $CuO/Ce_{0.8}Zr_{0.2}O_\delta$) favor the formation of surface bicarbonates in preference of carbonates, while catalysts with lower CO-PROX activity (X= La, Pr or Nd) accumulate more carbonates on the surface. It is known that the accumulation of carbon-containing species on CuO/CeO_2 PROX catalysts decreases the activity due to blockage

of active sites.[28] The positive effect on the CO oxidation rate of the presence of surface bicarbonates as adsorbed species with regards to carbonates could be related to the lower thermal stability of the former species, which would lead to a faster desorption of CO_2 leaving the surface available for further chemisorption of other potential species which might act as reaction intermediates. However, there is no experimental evidence to support this hypothesis, and it could also be possible that CO_2 produced at CuO-Ceria actives sites is transferred to hydroxyls in a further step, leaving the actives sites available again. In any case, formation of bicarbonates in preference to carbonates seems positive for CO oxidation.

Catalysts hydroxyls are involved in the formation of surface bicarbonates, as it is deduced from Figure 7 where the intensity of the bicarbonates band at 1395 cm^{-1} is plotted as a function of the area of the hydroxyls band (3600-2500 cm^{-1} range). Note that the area of the hydroxyls band shows negative values because hydroxyls are consumed during the reactions. Linear relationships between the consumption of hydroxyls and the formation of bicarbonates are observed for all catalysts suggesting that the two processes are related to each other.

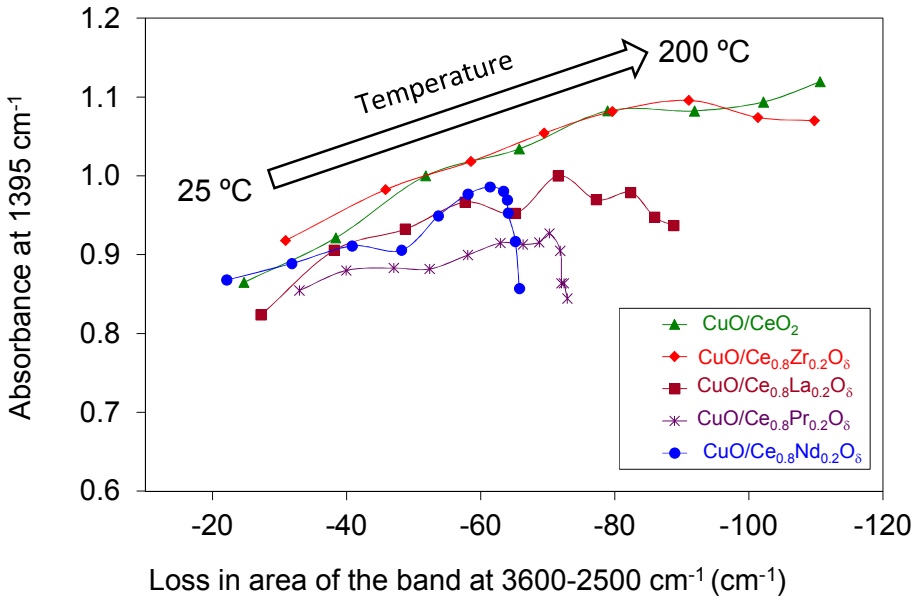

Figure 7. Relationship between bicarbonate formation (band at 1395 cm^{-1}) and hydroxyl consumption (band in the 2500-3600 cm^{-1} range).

Figure 7 also shows that the linear trend holds for the whole range of temperatures studied (25-200 ºC) for the most active catalysts (CuO/CeO_2 and $CuO/Ce_{0.8}Zr_{0.2}O_{\delta}$) but not for those with lower activity (X= La, Pr or Nd). Catalysts with X= La, Pr or Nd show a deviation from the trend line of Figure 7 above a certain temperature, and according to results in Figure 4b, this deviation occurs at a stage where the CO selectivity decreases, that is, where the onset of H_2 oxidation begin. A vertical drop in Figure 7 indicates that the amount of surface hydroxyls remains constant above a certain temperature while surface bicarbonates are depleted.

According to these results and the background literature, our proposed CO oxidation mechanism is as follows:

$2CuO + CO \rightarrow Cu_2O\text{-}O\text{-}CO$	step 1
$Cu_2O\text{-}O\text{-}CO + *\text{-}O \rightarrow Cu_2O + *\text{-}CO_3$	step 2a
$Cu_2O\text{-}O\text{-}CO + *\text{-}OH \rightarrow Cu_2O + *\text{-}CO_2OH$	step 2b
$Cu_2O + 1/2O_2 \rightarrow 2CuO$	step 3
$*\text{-}CO_3 \rightarrow *\text{-}O + CO_2$	step 4a
$*\text{-}CO_2OH \rightarrow *\text{-}OH + CO_2$	step 4b

where CuO are active sites for CO chemisorption at the copper oxide-cerium oxide interface, $Cu_2O\text{-}O\text{-}CO$ represents the Cu^{+}-CO carbonyl, *-O are chemisorption sites where surface carbonates ($*\text{-}CO_3$) are formed and *-OH are chemisorption sites where surface bicarbonates ($*\text{-}CO_2OH$) are formed.

The CO oxidation reaction mechanism starts with CO chemisorption at the copper oxide-cerium oxide interface and formation Cu^{+}-CO carbonyls (step 1), and it has been proposed that chemisorbed CO is oxidized to CO_2 following a Mars van Krevelen mechanism using the Cu^{2+}/Cu^{+} redox cycle.[15] Then, CO_2 is transferred from the copper oxide-cerium oxide interface to other surface sites, probably on the ceria support, forming bicarbonates (step 2a) and carbonates (step 2b), and molecular oxygen reoxidizes the reduced sites *via* steps 3. Surface hydroxyls are involved in the formation of bicarbonates (step 2b). Finally, CO_2 is desorbed following steps 4a and 4b.

3.4.2. Product poisoning versus Cu^{+}-CO carbonyl

The contribution to the CO oxidation rate of the copper oxide-cerium oxide interface reducibility and of the carbon products desorption has been analyzed.

Figure 8 shows the area of the Cu^{+}-CO carbonyl peak monitored under CO-PROX reaction conditions for all $CuO/Ce_{0.8}X_{0.2}O_{\delta}$ catalysts as a function of the reaction temperature, where it is observed that the room temperature formation of the Cu^{+}-CO carbonyl obtained with the Zr-containing catalyst is about three times higher to that formed on the undoped CuO/CeO_2 counterpart, and that the Cu^{+}-CO carbonyl formation is delayed to higher temperatures for catalysts with X = La, Pr or Nd.

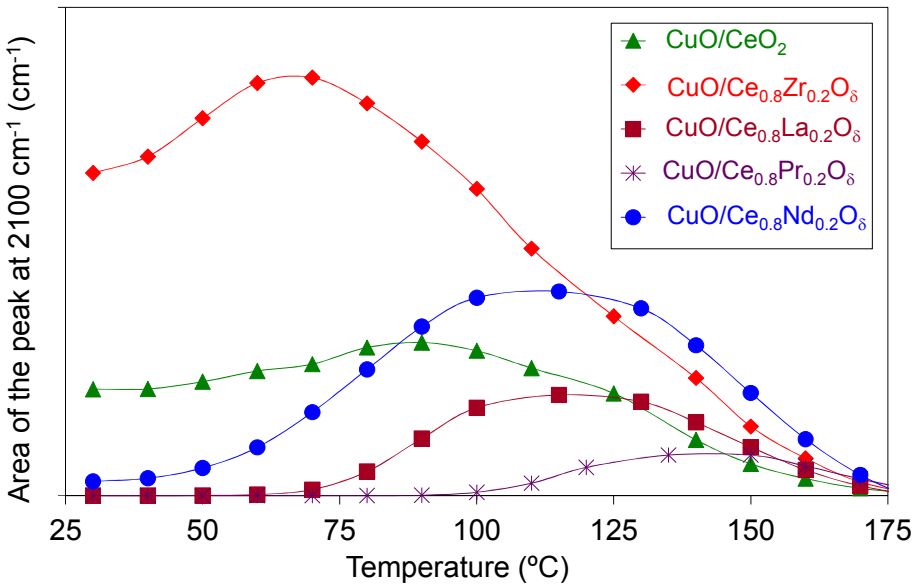

Figure 8. Integrated area of the Cu^{+}-CO carbonyl band at 2100 cm^{-1} as a function of the reaction temperature.

The temperature of maximum carbonyl coverage has been determined from Figure 8, and this temperatures correlate to the CO oxidation rates. Figure 9 shows the relationship between the CO oxidation rate and the formation of the Cu^{+}-CO carbonyl in the CO-PROX experiments. The data for most $CuO/Ce_{0.8}X_{0.2}O_{\delta}$ catalysts lie on a straight line, confirming the important role of the reducibility of the copper oxide-cerium oxide interface.[15,16]

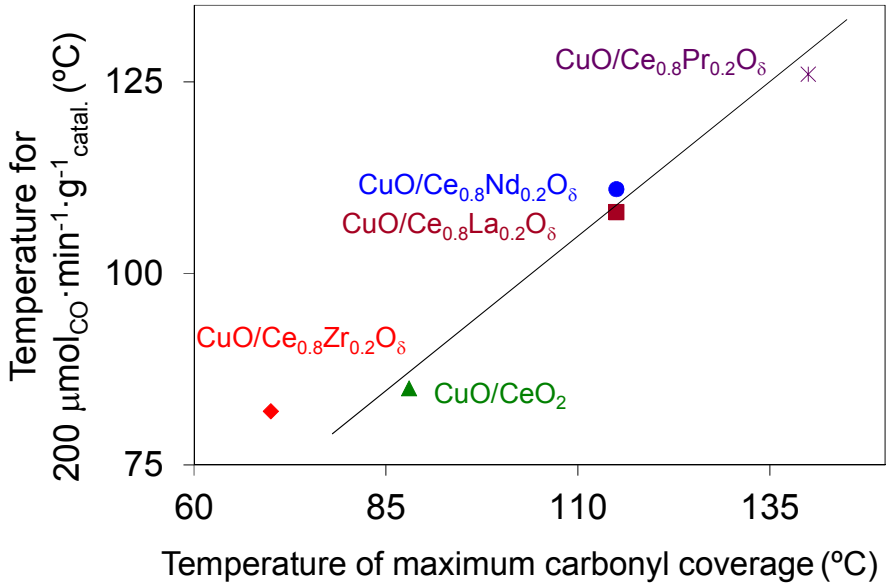

Figure 9. Relationship between temperature required to attain a certain CO oxidation rate and temperature corresponding to the maximum absorbance due to Cu^+-CO carbonyl.

However, the CO oxidation rate obtained with the Zr-containing catalyst is lower than that predicted by its Cu^+-CO carbonyl population. These results indicate that the Cu^+-CO carbonyl formation (step 1) is the rate limiting step for temperatures above a certain threshold (above 90 ºC approximately for the experimental conditions of this study) but, below this temperature, the accumulation of reaction products on the catalyst surface must also be taken into account because decomposition of reaction intermediates (steps 4a and 4b) becomes the slowest step of the mechanism. Therefore, the nature of the carbon species accumulated on the catalyst (bicarbonates or carbonates) should be mainly relevant below this temperature (90ºC).

The area of a broad DRIFTS band envelope with several contributions appearing in the 1650-1300 cm^{-1} range has been calculated. This band can be attributed to surface carbonates and

bicarbonates (and formates in particular cases). Figure 10 shows the area of this band as a function of the reaction temperature for all catalysts.

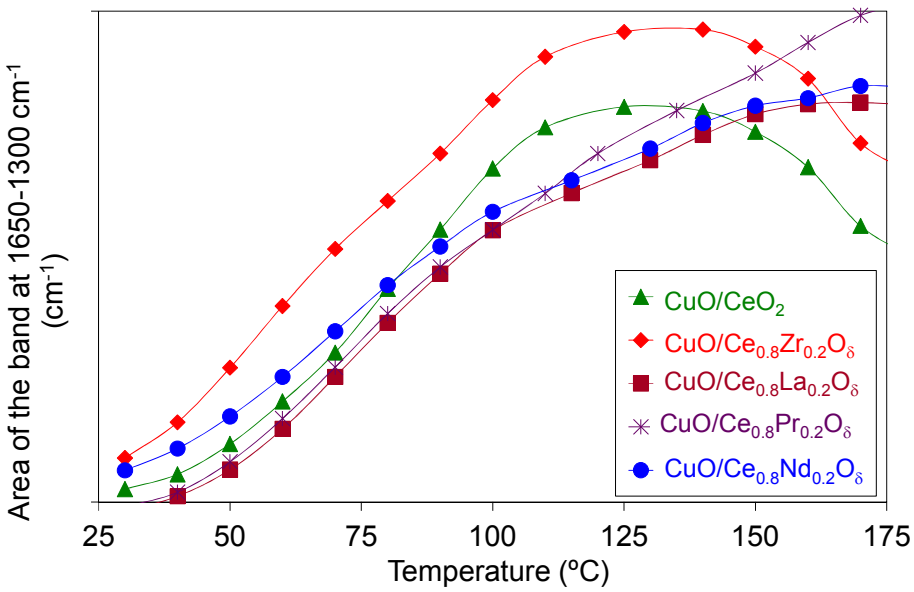

Figure 10. Integrated area of the band due to carbon containing products (carbonates + bicarbonates + formates) in the 1650-1300 cm^{-1} range as a function of the reaction temperature.

The accumulation of carbon containing reaction products is highest for the Zr-containing catalyst, its area of the 1650-1300 cm^{-1} band being, for instance, twice that of CuO/CeO_2 at 50 ºC. The poisoning by the formation of carbon containing adsorbed intermediates explains why the CO oxidation rate of the $CuO/Ce_{0.8}Zr_{0.2}O_\delta$ catalyst does not follow the trend predicted by the formation of the Cu^+-CO carbonyl (Figure 9). Comparison of the CuO/CeO_2 and $CuO/Ce_{0.8}Zr_{0.2}O_\delta$ behavior is interesting because both catalysts show similar CO-PROX activity,

the latter more readily forming the Cu^{+}-CO carbonyl at low temperature but also suffering much stronger inhibition by adsorbed products. Therefore, the contribution to the CO oxidation rate of the Cu^{+}-CO carbonyl formation and carbon products desorption oppose each other at low temperature. Taking the trend of Figure 9 into account, poisoning by reaction products becomes of special relevance at temperatures below ca. 90 ºC for the experimental conditions used in this study.

The CO-PROX experiments performed in this study show that ceria doping with foreign cations has either no effect or a negative impact on the activity, and this observation has been also reported by many authors.[29] There have been only reported few examples of improved CO-PROX activity of copper oxide-cerium oxide activity upon ceria doping,[30-32] but the reasoning why some authors observe the positive effect of ceria doping while most do not has not been fully explained. It has been proposed that the incorporation of foreign cations into the ceria lattice hinders the extent of copper oxide-cerium oxide interaction and it is this interface where the most active sites for CO oxidation are located.[33] Temperature programmed reduction experiments performed with H_2, (Figure 3), also indicate that the onset reduction temperature is lowest for the most active catalysts in the CO-PROX reaction (CuO/CeO_2 and $CuO/Ce_{0.8}Zr_{0.2}O_{\delta}$), that is, most dopants (X = La, Pr or Nd) retard CO oxidation with regard to CuO/CeO_2 and $CuO/Ce_{0.8}Zr_{0.2}O_{\delta}$ because they delay the onset in the reduction temperature.

3.4.3. Comparing CO-PROX with other catalytic reactions

The observed lack of influence or negative effect of ceria doping in the CO-PROX activity is in disagreement with the general behavior of ceria in most catalyzed reactions, such as in Three

Way Catalysts (TWC) where ceria doping by Zr^{4+} enhances the oxygen storage capacity, the redox properties, and overall, the catalytic performance.[34] The positive effect of ceria doping has been also reported for ceria-catalyzed diesel soot combustion[35,36] or NOx storage and Reduction (NSR) on Pt/Ceria catalysts,[37] for instance, where the redox properties of ceria play an important role.

An important difference between the CO-PROX reaction and the other applications where the doping of ceria has a positive effect is the range of temperatures where the reactions take place. Ceria doping with foreign cations usually has a positive effect on the activity for catalytic applications occurring at medium or high temperatures (around 200-300ºC for TWC and NSR or > 400 ºC for soot combustion, for instance). Dopants improve the thermal stability, oxygen storage capacity and/or some other physic-chemical properties of the ceria-based oxide, and therefore the catalytic activity, but the potential stabilization of the reaction intermediates on the catalyst has a minor effect on the reaction rate because the temperature is high enough to encourage desorption of the reaction products. On the other hand, the CO-PROX reaction takes place below ca 100ºC, and desorption of reaction products becomes a critical step. Therefore, the challenge for CO-PROX is to prepare copper oxide-cerium oxide catalysts which are readily reducible at low temperature but that, at the same time, also desorb the reaction products at low temperature, and the participation of catalyst hydroxyls in the formation of bicarbonates as reaction intermediates has a positive effect.

4.- Conclusions

The CO oxidation rate accelerated by copper oxide-cerium oxide catalysts in CO-PROX conditions correlates with the formation of the Cu^{+}-CO carbonyl above a critical temperature (90ºC for the experimental conditions of this study) because step 1 (copper carbonyl formation) is the rate limiting step. However, desorption of carbon containing products (steps 4a and 4b) is the slowest step below this threshold temperature. The hydroxyl groups on the catalyst surface play a key role in determining the nature of the carbon-based intermediates formed upon CO chemisorption and oxidation. Hydroxyls favor the formation of bicarbonates with respect to carbonates, and catalyst which preferentially form bicarbonates attain faster CO oxidation rates than those which favor carbonates.

Acknowledgments

The authors thank the financial support of Generalitat Valenciana (Project PROMETEOII/2014/010 and grant BEST/2014/250), the Spanish Ministry of Economy and Competitiveness (Projects CTQ2012-30703, CTQ2012-31762, MAT2014-61992-EXP and grant PRX14/00249), and the UE (FEDER funding).

Supporting Information. Consecutive catalytic tests in a fixed-bed reactor; selected m/z signals recorded during operando DRIFTS-MS experiments. This material is available free of charge *via* the Internet at http://pubs.acs.org.

Corresponding Author

*Inorganic Chemistry Department; University of Alicante. Carretera de San Vicente s/n. E03080, Alicante (Spain).Tel. (+34) 965903538; Fax. (+34) 965903454. Email: agus@ua.es

Author Contributions

The manuscript was written by contributions from all authors. All authors have given their approval to the final version of the manuscript. All authors contributed equally.

References

[1] Ghenciu, A. F. *Curr. Opin. Solid. St. M.* **2002**, 6, 389-399.

[2] Park, E.D.; Lee, D.; Lee, H.C. *Catal. Today* **2009**, 139, 280-290.

[3] Fu, Q.; Saltsburg, H.; Flytzani-Stephanopoulos, H. *Science* **2003**, 301, 935-938.

[4] Ko, E.-Y.; Park, E. D.; Lee, H. C.; Lee D.; Kim, S. *Angew. Chem., Int. Ed.* **2007**, 46, 734-737.

[5] Hornes, A.; Hungria, A. B.; Bera, P.; Lopez Cámara, A.; Fernandez-Garcia, M.; Martinez-Arias, A.; Barrio, L.; Estrella, M.; Zhou, G.; Fonseca, J. J.; Hanson, J. C.; Rodriguez, J. A. *J. Am. Chem. Soc.* **2010**, 132, 34-35.

[6] Tada, M.; Bal, R.; Mu, X.; Coquet, R.; Namba, S.; Iwasawa, Y. *Chem. Commun.* **2007**, 44, 4689-4691.

[7] Sedmak, G.; Hočevar, S.; Levec, J. *J. Catal.* **2003**, 213, 135-150.

[8] Wang, W.W.; Du, P.P.; Zou, S.H.; He, H.Y.; Wang, R.X.; Jin, Z.; Shi, S.; Huang, Y.Y.; Si, R.; Song, Q.S.; Jia, C.J.; Yan, C.H. *ACS Catal.* **2015**, 5, 2088−2099.

[9] Guzman, J.; Carrettin, S.; Corma, A. *J. Am. Chem. Soc.* **2005**, 127, 3286-3287.

[10] Deng, W.; Flytzani-Stephanopoulos, M. *Angew. Chem., Int. Ed.* **2006** 45, 2285-2289.

[11] Alayoglu S.; Eichhorn, B. *J. Am. Chem. Soc.* **2008**, 130, 17479-17486.

[12] Nilekar, A.U.; Alayoglu, S.; Eichhorn, B.; Mavrikakis, M. *J. Am. Chem. Soc.* **2010**, 132, 7418- 7428.

[13] Morfin, F.; Nassreddine, S.; Rousset, J.L., Piccolo, L. *ACS Catal.* **2012**, 2, 2161-2168.

[14] Zhang, R.; Haddadin, T.; Rubiano, D. P.; Nair, H.; Polster, C. S.; Baertsch, C. D. *ACS Catal.* **2011**, 1, 519–525.

[15] Gamarra, D.; Belver, C.; Fernández-García, M.; Martínez-Arias, A. *J. Am. Chem. Soc.* **2007**, 129, 12064-12065

[16] *Martínez-Arias, A.; Hungría, A. B.; Fernández-García, M.; Iglesias-Juez, A.; Soria, J.; Conesa, J. C.; Anderson, J. A.; Munuera, G. Phys. Chem. Chem. Phys.* **2012**, 14 2144-2151.

[17] Polster, C. S.; Nair, H.; Baertsch, C. D. *J. Catal.* **2009**, 266, 308-319.

[18] Liu, K.; Wang, A.; Zhang, T. *ACS Catal.* **2012**, 2, 1165–1178.

[19] van Berkum, J. G. M.; Delhez, R.; de Keijser, Th. H.; Mittemeijer, E. J. *Acta Cryst.* **1996**, A52, 730-747.

[20] Guillén-Hurtado, N.; Bueno-López, A.; García-García. A. *J. Mater. Sci.* **2012**, 47, 3204–3213.

[21] Krishna, K.; Bueno-López, A.; Makkee, M.; Moulijn. J.A. *Appl. Catal. B Env.* 75, **2007**, 189–200.

[22] Bueno-López, A.; Such-Basáñez, I.; Salinas-Martínez de Lecea, C. *J. Catal.* **2006**, 244, 102–112.

[23] Ikryannikova, L.N.; Aksenov, A.A.; Markaryan, G.L.; Muraveva, G.P.; Kostyuk, B.G.; Kharlanov, A.N.; Lunina, E.V. *Appl. Catal. A Gen.* **2001**, 210, 225-235.

[24] Mineshige, A.; Taji, T.; Muroi, Y.; Kobune, M.; Fujii, S.; Nishi, N.; Inaba, M.; Ogumi, Z. *Solid State Ionics* **2000**, 135, 481-485.

[25] Mcbride, J.R.; Hass, K.C.; Poindexter, B.D.; Weber, W.H. *J. Appl. Phys.* **1994**, 76, 2435-2441.

[26] Spanier, J.E.; Richard, R.D.; Robinson, D.; Zhang, F.; Chan, S.-W.; Herman, I.P. *Phys. Rev. B* **2001**, 64, 245407-245407-8.

[27] Fornasiero, P.; Di Monte, R.; Rao, G.R.; Kaspar, J.; Meriani, S.; Trovarelli, A.; Graziani, M. *J. Catal.* **1995**, 151, 168-177.

[28] Gamarra, D.; Martínez-Arias, A. *J. Catal.* **2009**, 263, 189–195.

[29] López, I.; Valdés-Solís, T.; Marbán, G. *Int. J. Hydrogen Energ.* **2008**, 33, 197-205.

[30] Santos Moura, J.; da Silva Lima Fonseca, J.; Bion, N.; Epron, F.; de Freitas Silva, T.; Guimarães Maciel, C.; Mansur Assaf, J.; do Carmo Rangel, M. *Catal. Today* **2014**, 228, 40-50.

[31] Moretti, E.; Storaro, L.; Talon, A.; Riello, P.; Infantes Molina, A.; Rodríguez-Castellón, E. *Appl. Catal. B Env.* **2015**, 168-169, 385-395.

[32] Gong, L.; Huang, Z.; Luo, L.; Zhang, N. *Reac. Kinet. Mech. Cat.* **2014**, 111, 489-504.

[33] Manzoli, R.; Di Monte, F.; Boccuzzi, S.; Coluccia; Kašpar, J. *Appl. Catal. B* Env. **2005**, 61, 192-205.

[34] Kaspar, J.; Fornasiero, P.; Graziani, M. *Catal. Today* **1999**, 50, 285-298.

[35] Bueno-López, A.; Krishna, K.; Makkee, M.; Moulijn, J. *J. Catal.* **2005**, 230, 237-248.

[36] Aneggi, E.; de Leitenburg, C.; Dolcetti, G.; Trovarelli, A. *Catal. Today* **2006**, 114, 40-47.

[37] Strobel, R.; Krumeich, F.; Pratsinis, S.E.; Baiker, A. *J. Catal.* **2006**, 243, 229-238.

Table of Contents Graphic